JOURNAL OF SOLID STATE CHEMISTRY **141,** 155–159 (1998)
ARTICLE NO. SC987935

An Air-Synthesized, Mixed-Valent Vanadium Tungsten Monophosphate with Intersecting Tunnels: $Cs_5VW_4O_9VO_4(PO_4)_4$

F. Berrah, A. Leclaire, A. Guesdon, M. M. Borel, J. Provost, and B. Raveau

Laboratoire CRISMAT, UMR 6508 associé au CNRS, ISMRA et Université de Caen, 6 Boulevard du Maréchal Juin, 14050 Caen Cedex, France

Received January 8, 1998; in revised form June 8, 1998; accepted June 23, 1998

A new mixed-valent vanadium tungsten monophosphate $Cs_5V_2W_4O_{13}(PO_4)_4$ has been synthesized in air in spite of the presence of V(IV). It crystallizes in the space group $Cmc2_1$ with $a = 14.948(1)$, $b = 20.008(2)$, and $c = 9.942(1)$ Å. Its original structure, built up from W_2O_{11} bioctahedra, P_2VO_{10} tritetrahedra units, and VO_5 pyramids, can be described from $[W_2P_2O_{13}]_\infty$ layers parallel to (100) interconnected through VO_4 tetrahedra and VO_5 pyramids. This open framework forms intersecting tunnels running along $\vec{a}$ and $\vec{c}$, where the Cs^+ cations are located. Bond strength–bond length calculations and magnetic measurements show that the electrons are localized, V(IV) sitting in the VO_5 pyramid, whereas the VO_4 tetrahedra and WO_6 octahedra are occupied by V(V) and W(VI), respectively.

INTRODUCTION

Transition metal phosphates have been extensively investigated over the past several years owing to the open character of their structure (for a review, see Refs. 1 and 2) and to their ability to present a mixed valence of the transition element. Thus they can be considered as potential materials for various applications such as heterogeneous catalysis, ionic conductivity, or molecular sieves.

In addition to the foregoing applications, the research of matrices for the storage of nuclear elements such as radioactive cesium calls attention to transition metal phosphates. In this respect, vanadium phosphates are of great interest, since several cesium vanadophosphates have been synthesized at temperatures ranging from 973 to 1173 K (3–8). Nevertheless, the synthesis of these oxides requires reducing conditions, vanadium being either trivalent (3–5) or tetravalent (5–8). Recently, a vanadium tungsten phosphate $Cs_3V_2W_2O_9(PO_4)_2$, characterized by the mixed valence V(V)–V(IV) has been isolated (9), suggesting that mixed frameworks of the systems V–W–P–O are susceptible to accommodate cesium. In the present paper, we report on a new cesium monophosphate, $Cs_5VW_4O_9(VO_4)(PO_4)_4$, characterized by a mixed valence of vanadium, V(IV)–V(V), entirely prepared in air and at low temperature (783 K).

EXPERIMENTAL

Crystal Growth and Chemical Synthesis

Single crystals of this phase were grown from a mixture of nominal composition $Cs_8V_4W_4P_8O_{45}$. The growth was performed in two steps: first $H(NH_4)_2PO_4$, $CsNO_3$, and WO_3 were mixed in adequate ratios according to the composition $Cs_8W_{3.67}P_8O_{35}$ and heated in a platinum crucible for 2 h at 673 K to decompose the ammonium phosphate and the cesium nitrate. The required amounts of V_2O_5 (2 mol) and tungsten (0.33 mol) were then added and the resulting mixture was sealed in an evacuated silica ampoule. It was heated at 783 K for 33 h, cooled at 10 K/h to 633 K, and finally quenched to room temperature. From the resulting product, some orange crystals were extracted. Their EDS analysis allowed the presence of silicon to be ruled out and led to the cationic composition $Cs_5V_2W_4P_4$, which was confirmed from the structure determination.

The synthesis of a pure powder of this new phosphate $Cs_5VW_4O_9(VO_4)(PO_4)_4$ is remarkable since it can be performed entirely in air in spite of the presence of V(IV) and at low temperature (783 K). The synthesis was performed in two steps. In a first step $H(NH_4)_2PO_4$, $CsNO_3$, and WO_3 were mixed in adequate proportions according to the ideal composition $Cs_5W_4P_4O_{24.5}$ and heated in air for 2 h at 673 K. Under these conditions tungsten keeps the maximum oxidation state W(VI), and we avoid a partial reduction of vanadium due to the decomposition of ammonium phosphate, which would be difficult to control. Then in the second step, the required amounts of VO_2 and V_2O_5 were added and the resulting mixture was heated in air at 783 K for 12 h and quenched to room temperature. For this temperature, vanadium keeps its initial tetravalent state.

The X-ray powder diffraction pattern of this new phase confirms its purity. It can be indexed in a monoclinic cell, in agreement with the single-crystal study (Table 1).

0022-4596/98 $25.00

TABLE 1
Summary of Crystal Data, Intensity Measurements, and Structure Refinement Parameters for $Cs_5VW_4O_9VO_4(PO_4)_4$

1. Crystal data	
Space group	$Cmc2_1$
Cell dimensions	$a = 14.948(1)$ Å
	$b = 20.008(2)$ Å
	$c = 9.942(1)$ Å
Volume (Å^3)	2973.6(4)
Z	4
ρ_{calc} (g cm^{-3})	4.668
2. Intensity measurements	
λ(Mo$K\alpha$) (Å)	0.71073
Scan mode	ω–θ
Scan width (deg)	$1.1 + 0.35 \tan\theta$
Slit aperture (mm)	$1.06 + \tan\theta$
Max θ (deg)	45
Standard reflections	3 measured every 3600 s
Measured reflections	6618
Reflections with $I > 3\sigma$	3100
3. Structure solution and refinement	
Parameters refined	207
Agreement factors	$R = 0.034$, $R_w = 0.033$
Weighting scheme	$w = 1/\sigma^2$
Δ/σ_{max}	< 0.005

TABLE 2
Atomic Positional and Isotropic Displacement Parameters

Atom	x	y	z	U_{eq} (Å^2)
W(1)	0.16982(3)	0.18908(2)	0.25000	0.00933(8)
W(2)	0.30915(3)	0.44019(2)	0.48619(6)	0.0150(1)
Cs(1)	$\frac{1}{2}$	0.29225(8)	0.4269(2)	0.0365(5)
Cs(2)	0.2444(1)	0.37240(6)	0.1283(1)	0.0387(3)
Cs(3)	0	0.02528(6)	0.2765(1)	0.0218(3)
Cs(4)	$\frac{1}{2}$	0.07862(8)	−0.0297(2)	0.0473(6)
V(1)	$\frac{1}{2}$	0.2902(1)	−0.0184(3)	0.0104(6)
V(2)	$\frac{1}{2}$	0.1038(2)	0.3526(5)	0.029(1)
P(1)	0.1865(2)	0.2954(1)	0.4916(3)	0.0092(6)
P(2)	0.3046(2)	0.0501(1)	0.2830(3)	0.0117(7)
O(1)	0.1085(6)	0.2529(5)	0.1831(9)	0.020(3)
O(2)	0.0919(6)	0.1604(4)	0.3754(9)	0.015(2)
O(3)	0.1465(6)	0.1233(5)	0.1191(9)	0.016(2)
O(4)	0.2776(6)	0.2188(4)	0.1326(9)	0.013(2)
O(5)	0.2328(5)	0.2456(4)	0.3915(9)	0.011(2)
O(6)	0.2636(7)	0.1143(4)	0.3261(9)	0.019(3)
O(7)	0.3727(7)	0.4094(5)	0.355(1)	0.028(3)
O(8)	0.3755(8)	0.5066(6)	0.535(1)	0.037(3)
O(9)	0.2254(8)	0.4930(5)	0.371(1)	0.032(3)
O(10)	0.2069(6)	0.3663(4)	0.4484(8)	0.016(2)
O(11)	0.2121(9)	0.4672(5)	0.6376(9)	0.037(4)
O(12)	$\frac{1}{2}$	0.3276(7)	0.123(1)	0.026(4)
O(13)	0.4135(5)	0.2153(4)	−0.011(1)	0.016(2)
O(14)	$\frac{1}{2}$	0.129(1)	0.506(3)	0.099(5)
O(15)	$\frac{1}{2}$	0.169(1)	0.255(3)	0.100(5)
O(16)	0.5931(7)	0.0500(6)	0.307(2)	0.065(6)

Single-Crystal X-Ray Diffraction Study

Single crystals were first selected optically and then tested by the Weissenberg method. The cell parameters were determined by diffractometric techniques at 293 K with a least-squares method based upon 25 reflections in the range $18° < \theta < 22°$.

An orange crystal with dimensions $0.114 \times 0.114 \times 0.064$ mm^3 was selected for the structure determination. The data were collected on a Enraf-Nonius CAD4 diffractometer with the parameters reported in Table 1. The reflections were corrected for Lorentz and polarization effects, for absorption, and for secondary extinction.

The Laue symmetry is *mmm* and the systematic extinctions $h + k = 2n + 1$ for all hkl and $l = 2n + 1$ for $h0l$ are consistent with the space groups C*mcm* and $Cmc2_1$. The Patterson function shows no Harker lines along $\vec{c}$, indicating that the space group is $Cmc2_1$. The structure was solved with the heavy-atom method. The refinement of the atomic coordinates and the anisotropic thermal factors of all the atoms led to $R = 0.034$ and $R_w = 0.033$ and to the atomic parameters listed in Table 2.

The calculations were performed on a SparcStation with the XTAL 3.2 program.

Magnetic Study

Magnetic susceptibility measurements were performed on a powder sample by SQUID magnetometry from 4.5 up to 300 K under 0.3 T after zero-field cooling, the magnetic field being applied after stabilization of the temperature at 4.5 K. The magnetic moment was then measured in increasing temperature up to 300 K.

RESULTS AND DISCUSSION

The projections of the structure of this new phosphate along $\vec{c}$ (Fig. 1) and $\vec{a}$ (Fig. 2) show the great diversity of the polyhedra which form the $[V_2W_4P_4O_{29}]_\infty$ host framework. The framework consists of corner-sharing PO_4 and VO_4 tetrahedra, WO_6 octahedra, and VO_5 pyramids. In this framework the WO_6 octahedra form bioctahedral W_2O_{11} units, whereas the PO_4 and VO_4 tetrahedra form tritetrahedral VP_2O_{10} units.

The important feature which characterizes this structure deals with the fact that this tridimensional framework can be described from the stacking along $\vec{a}$ of $[W_2P_2O_{13}]_\infty$ layers (Fig. 1) interconnected through VO_4 tetrahedra and VO_5 pyramids. In fact, the $[W_2P_2O_{13}]_\infty$ layers are very similar to the $[Mo_2P_2O_{13}]_\infty$ layers encountered in several molybdenum monophosphates, such as $A_3Mo_4O_6(PO_4)_4$ with $A =$ Rb and Tl (10), $Cs_3Mo_4O_6(PO_4)_4$ (11), and $A_2Mo_2O_3(PO_4)_2$ with $A =$ K, Rb, and Tl (12–14). In these layers (Fig. 3) the bioctahedral W_2O_{11} units are

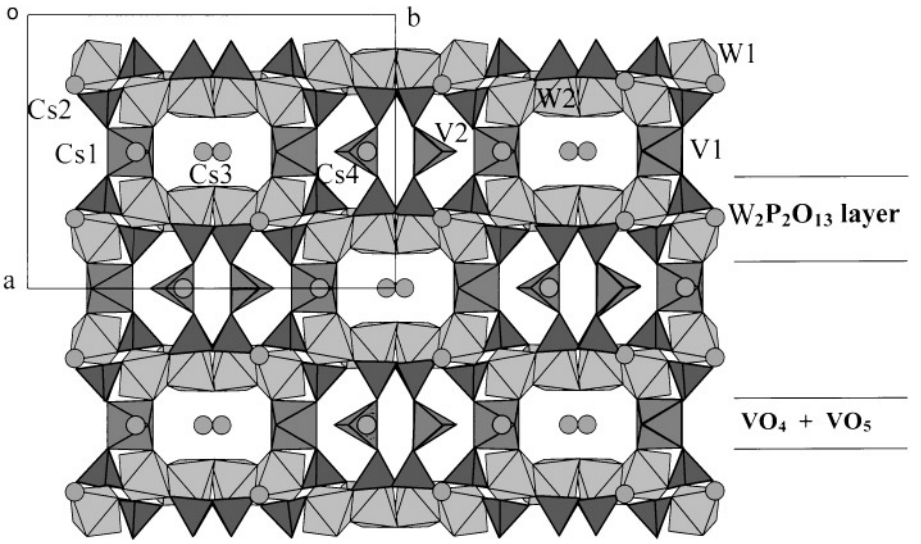

FIG. 1. Projection of the structure of $Cs_5VW_4O_9VO_4(PO_4)_4$ along $\vec{c}$.

interconnected through PO_4 groups forming eight-sided rings; within a layer each ring shares two polyhedra (one PO_4 tetrahedron and one WO_6 octahedron) with each of the four surrounding rings. Another interesting feature concerns the VP_2O_{10} tritetrahedral units, which are also observed in $Ba_2V_5O_8(PO_4)_4$ (15), where the corresponding VO_4 tetrahedron also ensures the connection between two rather dense layers, but which exhibits a different composition and geometry, $[V_4P_4O_{22}]_\infty$.

The interatomic distances and angles (Table 3) show that the PO_4 tetrahedra, which share their apices with three WO_6 octahedra and one VO_4 or one VO_5 pyramid, are rather regular.

The WO_6 octahedra are rather strongly distorted, with W–O distances ranging from 1.70 to 2.19 Å. The distortion is rather different for W(1) and W(2). W(1) exhibits one shorter W–O bond (1.707 Å) corresponding to its free apex, two intermediate W–O distances (1.80–1.844 Å) corresponding to the apices shared with V(1) and W(2), and three longer distances (2.035–2.185 Å) which form the W(1)–O–P bonds. For W(2), the two shorter W–O bonds (1.72–1.73 Å) correspond to the two free apices of the octahedron, the three longer ones (2.00–2.16 Å) characterize the three W(2)–O–P bonds, and the intermediate distance (1.948 Å) corresponds to the W(1)–O–W(2) bond.

The geometry of the VO_5 pyramid (V(1)) is characteristic of the vanadyl bond behavior, with one abnormally short V–O bond corresponding to the free apex of the pyramid, and four almost equal V–O bonds (1.98–2.00 Å) corresponding to the basal plane of the pyramid.

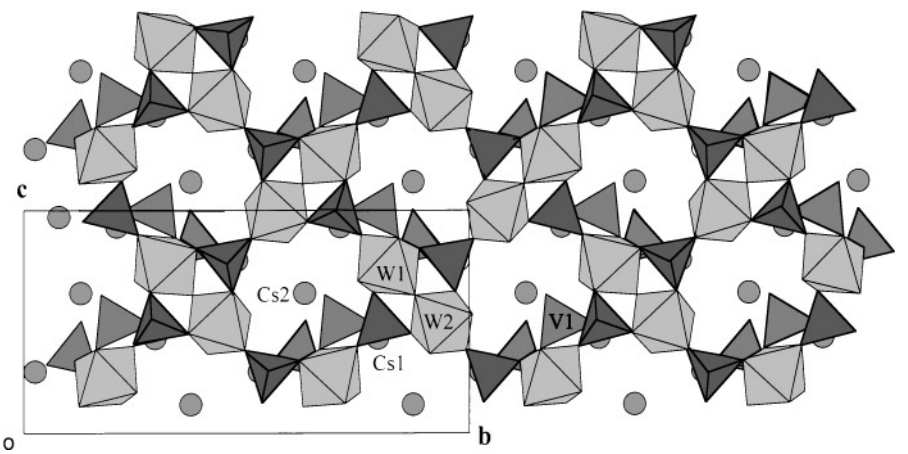

FIG. 2. Projection of the structure of $Cs_5VW_4O_9VO_4(PO_4)_4$ along $\vec{a}$.

TABLE 3
Distances (Å) and Angles (Deg) in the Polyhedra in $Cs_5VW_4O_9VO_4(PO_4)_4$

W(1)	O(1)	O(2)	O(3)	O(4)	O(5)	O(6)
O(1)	**1.707(9)**	2.67(1)	2.73(1)	2.67(1)	2.79(1)	3.88(1)
O(2)	99.3(4)	**1.800(9)**	2.78(1)	3.86(1)	2.71(1)	2.77(1)
O(3)	98.9(4)	97.8(4)	**1.884(9)**	2.74(1)	3.87(1)	2.71(1)
O(4)	89.0(4)	169.3(4)	87.4(4)	**2.077(9)**	2.71(1)	2.85(1)
O(5)	95.9(4)	89.9(4)	162.1(4)	82.6(3)	**2.036(9)**	2.75(1)
O(6)	172.6(4)	87.5(4)	83.1(4)	83.9(3)	81.1(3)	**2.19(1)**

W(2)	O(3)	O(7)	O(8)	O(9)	O(10)	O(11)
O(3)	**1.949(9)**	2.72(1)	2.75(1)	3.89(1)	2.78(1)	2.79(2)
O(7)	95.2(4)	**1.72(1)**	2.64(1)	2.77(2)	2.78(1)	3.87(2)
O(8)	96.6(5)	99.8(5)	**1.73(1)**	2.79(2)	3.87(1)	2.76(2)
O(9)	161.1(4)	95.8(5)	96.5(5)	**2.00(1)**	2.66(1)	2.71(1)
O(10)	85.0(4)	90.8(4)	169.0(5)	79.6(4)	**2.159(9)**	2.76(1)
O(11)	85.4(4)	170.2(5)	89.8(5)	81.2(4)	79.5(4)	**2.16(1)**

V(1)	O(2)	O(2)	O(12)	O(13)	O(13)
$O(2)^{iii}$	**2.00(1)**	2.75(1)	2.83(2)	2.74(2)	3.82(1)
$O(2)^{ii}$	87.0(4)	**2.00(1)**	2.83(2)	3.82(1)	2.74(1)
O(12)	103.5(4)	103.5(4)	**1.59(1)**	2.91(2)	2.91(2)
O(13)	86.9(3)	147.7(4)	108.7(5)	**1.980(8)**	2.59(2)
$O(13)^{vi}$	147.7(4)	86.9(3)	108.7(5)	81.5(3)	**1.980(8)**

V(2)	O(14)	O(15)	O(16)	$O(16)^{vi}$
O(14)	**1.61(3)**	2.63(5)	2.89(3)	2.89(3)
O(15)	109(2)	**1.63(3)**	2.81(3)	2.81(3)
O(16)	114.8(8)	109.1(8)	**1.82(1)**	2.78(2)
$O(16)^{iv}$	114.8(8)	109.1(8)	100.1(6)	**1.82(1)**

P(1)	$O(4)^{i}$	O(5)	O(10)	$O(13)^{i}$
$O(4)^{i}$	**1.528(9)**	2.51(1)	2.51(1)	2.48(1)
O(5)	108.0(5)	**1.569(9)**	2.51(1)	2.52(1)
O(10)	111.3(5)	109.1(5)	**1.513(9)**	2.46(1)
$O(13)^{i}$	109.5(5)	109.7(5)	109.2(5)	**1.511(8)**

P(2)	O(6)	$O(9)^{viii}$	$O(11)^{iii}$	$O(16)^{vi}$
O(6)	**1.49(1)**	2.42(1)	2.51(1)	2.51(2)
$O(9)^{viii}$	111.3(6)	**1.51(1)**	2.46(1)	2.37(2)
$O(11)^{iii}$	114.0(6)	109.5(6)	**1.51(1)**	2.47(2)
$O(16)^{vi}$	111.4(7)	101.8(7)	108.2(8)	**1.55(1)**

$Cs(1)–O(15) = 3.00(3)$
$Cs(1)–O(12) = 3.10(1)$
$Cs(1)–O(7)^{vi} = 3.10(1)$
$Cs(1)–O(7) = 3.10(1)$
$Cs(1)–O(1)^{ii} = 3.15(1)$
$Cs(1)–O(1)^{i} = 3.15(1)$
$Cs(1)–O(3)^{i} = 3.36(1)$
$Cs(1)–O(3)^{ii} = 3.36(1)$
$Cs(1)–O(14) = 3.37(3)$
$Cs(3)–O(8)^{x} = 3.10(1)$
$Cs(3)–O(8)^{iii} = 3.10(1)$
$Cs(2)–O(6)^{iii} = 3.02(1)$
$Cs(2)–O(7) = 3.05(1)$
$Cs(2)–O(4) = 3.11(1)$
$Cs(2)–O(1) = 3.18(1)$
$Cs(2)–O(10) = 3.23(1)$
$Cs(2)–O(8)^{ix} = 3.25(1)$
$Cs(2)–O(11)^{ix} = 3.25(1)$
$Cs(2)–O(5)^{iii} = 3.35(1)$
$Cs(2)–O(9) = 3.42(1)$
$Cs(4)–O(13) = 3.03(1)$
$Cs(4)–O(13)^{vi} = 3.03(1)$

TABLE 3—*Continued*

$Cs(3)–O(7)^{vii} = 3.10(1)$
$Cs(3)–O(7)^{viii} = 3.10(9)$
$Cs(3)–O(2) = 3.19(1)$
$Cs(3)–O(2)^{v} = 3.19(1)$
$Cs(3)–O(8)^{vii} = 3.20(1)$
$Cs(3)–O(8)^{viii} = 3.20(1)$
$Cs(3)–O(3) = 3.33(1)$
$Cs(3)–O(3)^{v} = 3.33(1)$
$Cs(4)–O(10)^{iii} = 3.29(1)$
$Cs(4)–O(10)^{iv} = 3.29(1)$
$Cs(4)–O(16)^{xi} = 3.35(1)$
$Cs(4)–O(16)^{xii} = 3.35(1)$
$Cs(4)–O(15) = 3.36(1)$

[a] Symmetry codes: i, $-x+\frac{1}{2}, -y+\frac{1}{2}, z+\frac{1}{2}$; ii, $x+\frac{1}{2}, -y+\frac{1}{2}, z+\frac{1}{2}$; iii, $-x+\frac{1}{2}, -y+\frac{1}{2}, z-\frac{1}{2}$; iv, $x+\frac{1}{2}, -y+\frac{1}{2}, -\frac{1}{2}+z$; v, $-x, y, z$; vi, $-x+1, y, +z$; vii, $x-\frac{1}{2}, y-\frac{1}{2}, z$; viii, $-x+\frac{1}{2}, y-\frac{1}{2}, z$; ix, $x, -y+1, z-\frac{1}{2}$; x, $x-\frac{1}{2}, -y+\frac{1}{2}, z-\frac{1}{2}$; xi, $x, -y, z-\frac{1}{2}$; xii, $-x+1, -y, z-\frac{1}{2}$.

The VO_4 tetrahedron (V(2)) exhibits two shorter V–O distances (1.61–1.63 Å) corresponding to its two free apices and two longer ones (1.82 Å) which form the V–O bonds of the VP_2O_{10} tritetrahedral units.

The cesium cations are distributed over four types of sites which are all fully occupied. Cs(2) is located within the $[W_2P_2O_{13}]_\infty$ layers, at the center of the eight-sided ring (Fig. 3), i.e., on the axis of the tunnels running along $\vec{a}$ (Fig. 2). In contrast, Cs(1), Cs(3), and Cs(4) are all located between the $[W_2P_2O_{13}]_\infty$ layers, at the level of the VO_5 pyramid and VO_4 tetrahedron (Fig. 1). Cs(3) sits near the axis of the tunnel running along $\vec{c}$, whereas Cs(4) and Cs(1) are located between the VO_4 tetrahedra and the VO_5 pyramids along $\vec{c}$, respectively. It is remarkable that, whatever the positions, one observes Cs–O distances larger than 3 Å (Table 3), which emphasizes the open character of this structure. This result is in agreement with the thermal factor values after refinement, which are rather high, ranging from 2.18 to 4.73 $Å^2$ Thus the coordination of cesium is difficult to define: it can be considered as ranging from seven to ten,

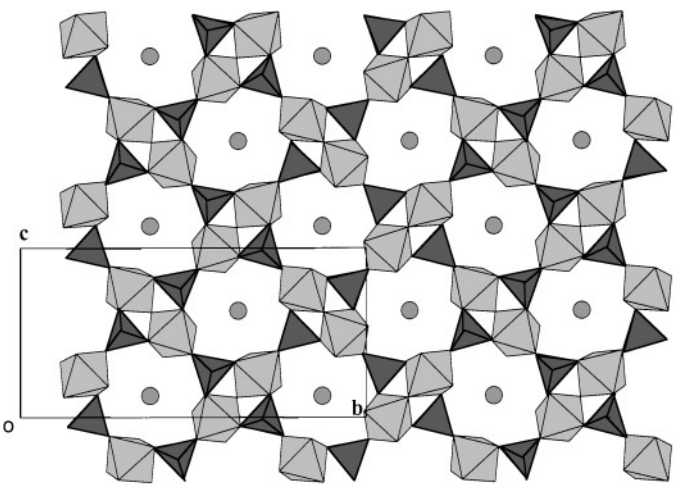

FIG. 3. A $[W_2P_2O_{13}]$ layer veiwed in projection along $\vec{a}$.

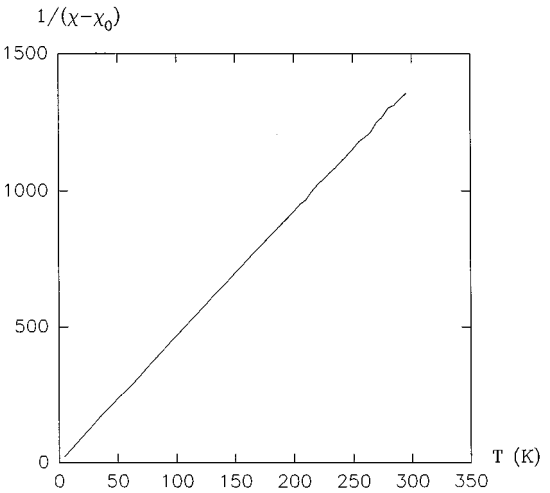

FIG. 4. Inverse molar magnetic susceptibility versus T.

if one admits that Cs–O bonds exist for distances between cesium and oxygen smaller than 3.5 Å.

Electronic Localization

From the interatomic distances, an electronic localization appears as most likely, with hexavalent tungsten sitting in octahedral sites, whereas the VO_4 tetrahedra and VO_5 pyramids should be occupied by pentavalent and tetravalent vanadium, respectively. The bond strength–bond length calculations (16) strongly support this hypothesis. One obtains indeed valences of 6.156, 6.176, 3.977, and 4.974 for W(1), W(2), V(1), and V(2), respectively.

The inverse molar susceptibility $\chi_m^{-1}(T)$ established after correction of the sample holder signal, was fit with a Curie–Weiss type law $\chi_m = \chi_0 + C_m/(T - \theta)$ (Fig. 4), leading to an effective magnetic moment of 1.32 μ_B per V(IV) and to $\theta = -1.33$ K for $\chi_0 = -0.0001$. This value of the effective magnetic moment is significantly lower than the theoretical moment, which is 1.73 μ_B for V(IV). Since the $V(IV)O_5$ pyramids share two of their apices with two W_2O_{11} bioctahedral units, this difference could be attributed to the existence of the interactions between the atoms of the VW_4O_{25} pentapolyhedral units resulting from this assemblage as shown in the molybdenum phosphates (17). Molecular orbital calculations will be carried out to verify this hypothesis by studying the nature of the electronic levels in this pentapolyhedral structural unit.

ACKNOWLEDGMENT

The authors acknowledge E. Canadel (U.A.B. Barcelona) for the molecular orbital calculations.

Note added in proof. Molecular orbital calculations have been carried out which confirm the occupancy of VO_4 tetrahedra and VO_5 pyramids by V^{5+} and V^{4+} respectively. They also evidence a partial delocalization of the electron of V(1) on W(1)O_6 octahedra of the $V(1)W(1)_2W(2)_2O_{25}$ unit.

REFERENCES

1. M. M. Borel, M. Goreaud, A. Grandin, Ph. Labbé, A. Leclaire, and B. Raveau, *Eur. J. Solid State Inorg. Chem.* **28,** 93 (1991).
2. C. N. R. Rao and B. Raveau, "Transition Metal Oxides." VCH, New York, 1995.
3. A. V. Laurov, V. P. Nikolaev, G. G. Sadikov, and M. Ya. Voitenkov, *Dokl. Akad. Nauk SSSR* **259,** 103 (1980).
4. B. Klinkert and M. Jansen, *Z. Anorg. Allg. Chem.* **567,** 87 (1988).
5. Y. P. Wang and K. H. Lii, *Acta Crystallogr., Sect. C* **45,** 1210 (1989).
6. K. H. Lii, Y. P. Wang, and S. L. Wang, *J. Solid State Chem.* **80,** 127 (1989).
7. K. H. Lii and S. L. Wang, *J. Solid State Chem.* **82,** 239 (1989).
8. K. H. Lii and W. C. Liu, *J. Solid State Chem.* **103,** 38 (1993).
9. F. Berrah, D. Mezaoui, A. Guesdon, M. M. Borel, A. Leclaire, J. Provost, and B. Raveau, *Chem. Mater.* **10,** 543 (1998).
10. M. M. Borel, A. Leclaire, A. Guesdon, and B. Raveau, *J. Solid State Chem.* **112,** 15 (1994).
11. M. M. Borel, A. Leclaire, A. Grandin, and B. Raveau, *J. Solid State Chem.* **108,** 336 (1994).
12. C. Gueho, M. M. Borel, A. Grandin, A. Leclaire, and B. Raveau, *J. Solid State Chem.* **104,** 202 (1993).
13. A. Guesdon, A. Leclaire, M. M. Borel, A. Grandin, and B. Raveau, *Acta Crystallogr., Sect. C* **50,** 1852 (1994).
14. A. Guesdon, M. M. Borel, A. Grandin, A. Leclaire, and B. Raveau, *Acta Crystallogr., Sect. C* **49,** 1877 (1993).
15. M. M. Borel, A. Leclaire, J. Chardon, and B. Raveau, *J. Mat. Chem.* **8,** 693 (1998).
16. N. E. Brese and M.O'Keeffe, *Acta Crystallogr., Sect. C* **47,** 192 (1991).
17. E. Canadell, J. Provost, A. Guesdon, M.-M. Borel, and A. Leclaire, *Chem. Mater.* **9,** 68 (1997).